PAPER

Observation of energetic terahertz pulses from relativistic solid density plasmas

New Journal of Physics
The open-access journal for physics

Observation of energetic terahertz pulses from relativistic solid density plasmas

A Gopal[1,2,7], T May[3], S Herzer[1], A Reinhard[3], S Minardi[4], M Schubert[3], U Dillner[3], B Pradarutti[5], J Polz[1,2], T Gaumnitz[1], M C Kaluza[1,2], O Jäckel[1,2], S Riehemann[5], W Ziegler[1], H-P Gemuend[6], H-G Meyer[3] and G G Paulus[1,2]

[1] Institute of Optics and Quantumelectronics, Friedrich-Schiller-Universität Jena, Max-Wien-Platz 1, 07743 Jena, Germany
[2] Helmholtz Institute Jena, Helmholtzweg 4, 07743 Jena, Germany
[3] Institut für Photonische Technologien, Postfach 100239, 07702 Jena, Germany
[4] Institute of Applied Physics, Friedrich-Schiller-Universität Jena, Max-Wien-Platz 1, 07743 Jena, Germany
[5] Fraunhofer Institut für Angewandte Optik und Feinmechanik, Albert-Einstein-Strasse 7, 07745 Jena, Germany
[6] Max Planck Institute for Radio Astronomy, Auf dem Huegel 69, 53121 Bonn, Germany
E-mail: amrutha.gopal@uni-jena.de

New Journal of Physics **14** (2012) 083012 (11pp)
Received 15 February 2012
Published 10 August 2012
Online at http://www.njp.org/
doi:10.1088/1367-2630/14/8/083012

Abstract. We report the first experimental observation of terahertz (THz) radiation from the rear surface of a solid target while interacting with an intense laser pulse. Experimental and two-dimensional particle-in-cell simulations show that the observed THz radiation is mostly emitted at large angles to the target normal. Numerical results point out that a large part of the emission originates from a micron-scale plasma sheath at the rear surface of the target, which is also responsible for the ion acceleration. This opens a perspective for the application of THz radiation detection for on-site diagnostics of particle acceleration in laser-produced plasmas.

[7] Author to whom any correspondence should be addressed.

Contents

1. Introduction

Plasmas produced by high-power (10^{12}–10^{15} W) lasers are unique laboratories for the investigation of matter at high density and temperature, such as those found in astrophysical environments [1, 2]. Besides the relevance to fundamental physics, hot laser plasmas have the potential for innovative applications ranging from generation of coherent electromagnetic radiation [3, 4] to the acceleration of charged particles with table-top-size settings [5, 6]. Progress in the investigation of both fundamental and applied aspects of hot laser plasmas necessarily requires powerful diagnostic tools to understand and eventually control their complex dynamics. In this context, characterization of laser plasmas using external probes is challenging because of the small spatio-temporal scales involved (a few tens of microns in space and several hundreds of picoseconds in time) [7]. A promising alternative is represented by the analysis of radiation generated by the internal dynamics of hot plasmas [8–10]. For instance, the higher-order harmonic radiation generated during laser–plasma interaction provides details of the electron dynamics at the critical density surface and related nonlinear optical effects in the plasma [10–12]. To date, studies of self-emitted radiation were mainly focused in the short-wavelength range [13] suitable to understand the electron dynamics happening on a short time scale [9]. Terahertz (THz) radiation from laser-produced plasmas in gases has been observed by various groups [14–17]. However, limited work has been reported on the observation of THz radiation from high-power laser-produced plasmas in solids [18–20]. In the earliest study, the generation of linearly polarized infrared radiation emitted from a solid target was attributed to a ponderomotively induced space-charge field [18]. The authors observed peak THz emission in the specular reflection direction of the incident laser pulse. The recent observation of THz radiation from the front surface of a solid target by Sagisaka *et al* [19] led them to propose the antenna mechanism, where the electrons generated by the laser pulse moving along the target surface emit THz radiation. The polarization of the emitted radiation is similar to that of the incident laser pulse. Previous observations were all from the front surface of the target where the high-power laser pulse impinges, and hence can be related to the electron dynamics. However, emission from the rear surface does not directly link to the incident laser pulse or to the THz radiation generated at the front surface as it is not able to travel through the dense solid plasma. Moreover, the radiation from the electrons exiting the rear surface falls mainly in the optical or in the high-frequency regime [21–23]. Therefore, the observation of THz radiation from the rear

side of the target should account for the ion acceleration process, where the transient dynamics of the accelerating sheath field acts as a source.

In this paper, we report the first observation of self-generated non-collinear THz pulses from the rear surface of a solid target during relativistic laser–solid interaction. No less than 2 μJ of radiation with frequency between 0.15 and 2 THz was measured by focusing 30 TW (terawatt) femtosecond laser pulses at relativistic intensities onto a thin titanium foil. Our experiments and two-dimensional (2D) particle-in-cell (PIC) simulations show that the measured THz radiation is emitted from the rear surface of the target, predominantly at large angles with respect to the target normal. Furthermore, the numerical results and experiment indicate that a substantial fraction of the observed radiation is linked to the dynamics of the ion acceleration process at the rear surface of the laser-irradiated target.

1.1. Experimental setup

The experiment was performed using the 30 TW JETI (JEna TI-Sapphire) laser system at the Institute of Optics and Quantum Electronics at the University of Jena. The JETI laser delivers 1.0 J, 800 nm and 30 fs pulses at a 10 Hz repetition rate. A schematic diagram of the experimental setup is shown in figure 1. P-polarized laser pulses were used to irradiate 5 μm thick titanium foils placed inside the experimental vacuum chamber. The laser beam was focused to a peak intensity of 10^{19} W cm^{-2} using an off-axis parabolic mirror with 12 cm focal length. In order to collect the THz radiation emitted in the perpendicular direction to the target normal, a metallic ellipsoidal mirror (f-number = 1.18) was employed. The target and the focal point of the laser pulse were located at the first focus of the ellipsoidal mirror, oriented with its semi-major axis perpendicular to the target surface. The target holder was designed in such a way that no radiation emitted from the target front surface entered our collection optics. The ellipsoidal mirror was designed to collect THz radiation emitted from the rear surface of the target at elevations between 0° and 41° (equivalent to a solid angle of 4.12 sr), and refocus it at the second focus of the ellipse. Here, a motorized iris diaphragm (max. diameter 34 mm) was placed to scan the radial intensity distribution of the THz radiation. This design rejects efficiently the radiation emitted in the forward direction (in target normal direction) and within the field of view of the iris (±4° at full aperture, corresponding to a solid angle of 10^{-3} sr). Behind the iris diaphragm, a collimation off-axis parabola and a sequence of plane mirrors were used to relay the THz radiation through a Zeonex window onto a calibrated hybrid pyroelectric Joule meter [24], placed outside the vacuum chamber. The detector was coated with organic black material to extend the sensitivity to a large spectral window ranging from 0.1 to 30 THz. Detection of parasitic electromagnetic radiation (such as laser light, background radiation, etc) and signal saturation was prevented by means of suitable calibrated filters and attenuators placed in front of the detector. Along with the THz radiation, the ion spectra were recorded simultaneously by means of a Thomson parabola detector, thanks to a 3 mm hole drilled in the center of the T-ray collimation parabola. The focusing of the laser pulse was tuned to ensure the maximum ion energy and number.

2. Results

The optical components in the beam path were calibrated using a Fourier transform infrared spectrometer. By accounting for the transmission/reflection of each optical component in the beam relay path, the readout of the detector could be used to measure the absolute energy

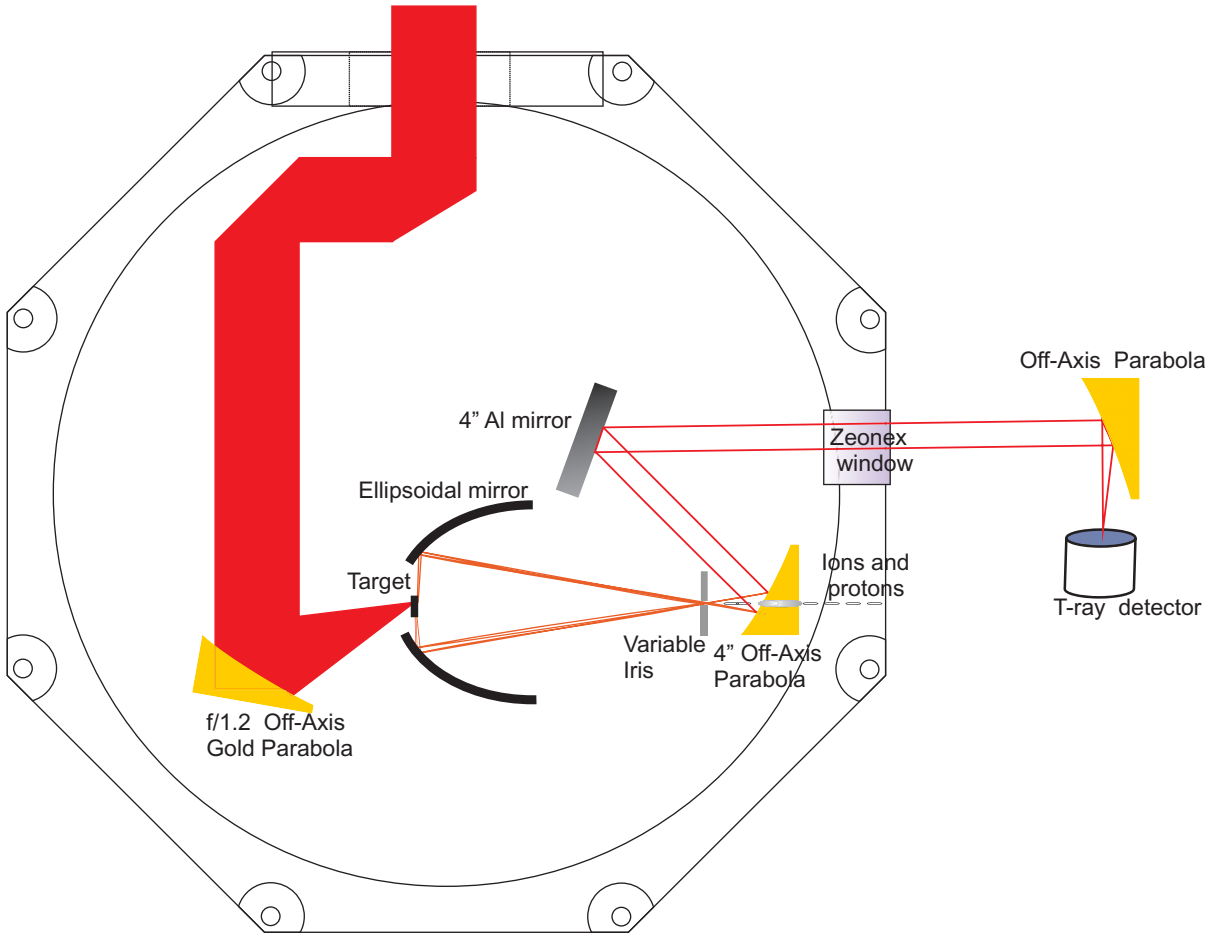

Figure 1. Schematic diagram of the experimental setup. TW laser pulses were focused onto a 5 μm thick titanium foil using a 45° off-axis parabolic mirror. THz emitted non-collinearly from the rear surface was collected using a metallic ellipsoidal mirror and was focused onto the pyroelectric detector placed outside the vacuum chamber.

of the THz radiation generated during the experiment. For incident laser energies of 650 mJ (estimated intensity—10^{19} W cm^{-2}), we detected T-ray pulses with energy not less than 2 μJ in the 0.15–2 THz band. Considering the coupling losses in the beam relay system the actual emitted energy should be an order higher than the measured signal. Assuming that the THz radiation is a single optical cycle pulse the peak power of the radiation should be above 2 MW. In addition, the polarization of the THz radiation was measured using wire grid polarizers. The signal level reduced to half when a wire grid polarizer was placed in front of the detector. This shows that the observed THz is radially polarized (as expected from a dipole emission) or unpolarized.

2.1. Spectral analysis

The spectral analysis of the T-rays was performed using a collection of lowpass and bandpass filters. The bandpass filters are a combination of bandpass/lowpass filters; they are exact

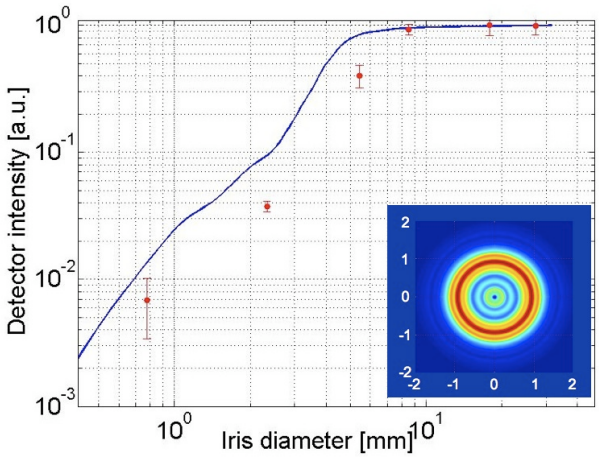

Figure 2. Spatial distribution of THz radiation at the iris diaphragm. Numerical simulation of the spatial distribution of THz radiation for various iris diameters (blue line). Experimentally measured spatial distribution of the THz radiation for various iris diameters (red diamonds). Inset: simulated effective 2D spatial distribution of THz radiation behind (5 mm) the iris. The distribution clearly shows that the emission is strongly non-collinear.

replicas of the far infrared filters used on the ISOPHOT instrument [25]. The lowpass filters are commercially available and are made of wire grids of various diameters and separation. The filters were placed in front of the detector. The observed T-ray signal contained spectral information for frequencies between 0.15 and 2 THz (which was the cut-off frequency of the attenuators and the chamber window). The spectral analysis shows that about 60% of the total detected energy is distributed in the 0.6–0.9 and 1.6–2 THz regions. Only 30% of the transmitted energy is between 0.3 and 0.6 THz.

2.2. Spatial distribution

The spatial distribution of the collected THz radiation was measured by recording the transmitted signal for various apertures of the iris diaphragm at the second focus of the ellipsoidal mirror. The bi-logarithmic plot of figure 2 shows that for iris diameters d smaller than 8 mm the measured signal strength scales as d^3. For larger apertures, the signal is nearly constant, indicating that almost the entire energy of the focused T-ray beam is distributed within a radius of 4 mm. The power-law scaling shows that the center of the THz beam is hollow rather than filled. Because the spatial spectrum of a hollow beam has peaks off-axis, our observation is compatible with non-collinear THz emission. The spectral content of the THz radiation from the experiments is used to simulate the expected detected signal behind the iris diaphragm. The best fit is represented by the blue line of the plot in figure 2. The effective spatial distribution of the THz radiation behind the iris is shown in the inset of figure 2. In the simulation we assumed that the observed pattern has a radial polarization state, as expected from dipole emission. Despite a small quantitative mismatch between the experiment and the numerical simulation, the power-law trend is accurately reproduced by the numerical model.

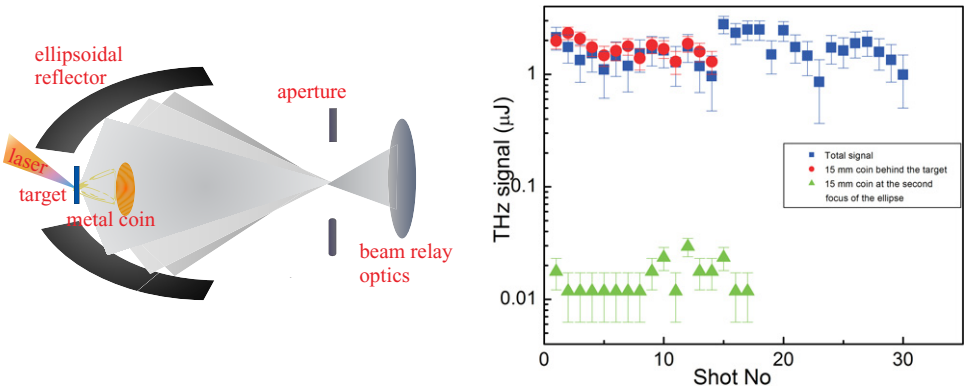

Figure 3. A metal coin of 15 mm diameter placed 10 mm behind the target confirmed the directionality of the measured T-rays. Blue squares of the data plot indicate the T-ray signal without the metal coin. Red dots represent the shots with coin just behind the target. Green triangles show the T-rays present when the coin was placed at the second focus of the ellipsoidal mirror. Error bars indicate the shot-to-shot fluctuation.

Additional measurements were carried out by placing a metal coin of diameter 15 mm behind the target at a distance of 10 mm so that all the forward emitted radiation is blocked (see figure 3). Such an arrangement would cast a shadow cone of base diameter 18 cm on the iris, hence blocking all the forward emitted radiation. Moreover, the geometry of the beam block is such that the reflected THz radiation from the coin back to the target will propagate at elevation angles larger than 54°, and thus cannot be reflected by the ellipsoidal mirror inside the iris. The THz detector placed outside the vacuum chamber did not observe any significant change in the energy of the THz radiation. In contrast, when the metal coin was placed at the second focus of the ellipsoidal mirror the signal on the THz detector vanished to the background level. These tests show unequivocally that the radiation is emitted at elevation angles between 0° and 41° and corroborate the interpretation of the aperture scanning measurements.

2.3. Particle-in-cell simulations

In order to identify the source of the THz radiation, we performed 2D PIC simulations [26]. A simulation box of $20\,\mu\text{m} \times 200\,\mu\text{m} \times 100\,\mu\text{m}$ in the x-, y- and z-directions, respectively, and a spatial resolution of 50 nm was used together with absorbing boundary conditions. An aluminum target $1\,\mu$m thick, $10\,\mu$m wide and $30\,\mu$m long was placed $25\,\mu$m from the entrance plane (xy) of the simulation box. The code calculates the field ionization rates and can handle populations of neutral and ionized Al atoms. The focused intensity of the laser was $1.3 \times 10^{19}\,\text{W cm}^{-2}$ and the density was $6 \times 10^{22}\,\text{cm}^{-3}$. The laser pulse was polarized in the plane perpendicular to the plane of incidence and propagating in the z-direction had a central wavelength of 800 nm. For the evaluation of the THz field we chose a 2D simulation plane along the y–z-direction in the center of the simulation box (see figure 4(b)). In order to measure the THz radiation field lineout was taken on a semicircle of $30\,\mu$m radius from the center of the target rear surface. The fields were extracted every 1.44 fs for a total duration of 738 fs. The retrieved spatio-temporal field structure was Fourier transformed in time and filtered to reject optical frequencies. In order to make sure that the observed field can propagate as

radiation, the Poynting vectors were plotted. The radiation was selected in frequency using a lowpass filter with a hard cut-off at 25 THz. A suitable timeframe was chosen to observe dipole-like emission. A more extended spatial emission can be observed for temporally integrated emission, which is due to the hot electrons or the surface plasmons traveling along the target surface. The magnitude of the isotropic emission is much smaller/negligible when the number of particles per cell is reduced by a factor of 7, a clear indication that the dipole field is due to the plasma sheath at the rear surface of the target, which is accelerating the positive charges.

Upon hitting the target at $t = 80$ fs (time elapsed from the beginning of the simulation), the femtosecond pulse completely ionizes the aluminum atoms and excites a low-frequency, expanding electromagnetic wave at the back of the target. The radiation flux is visualized in figure 4(a), where a snapshot (at $t = 194$ fs) of the magnitude and direction of the Poynting vector is shown. The emitted radiation has a rather complex spatio-temporal structure whose analysis revealed the existence of three main mechanisms, each responsible for the generation of THz radiation featuring characteristic spatio-temporal and spectral signatures. The fields are represented in normalized quantities. The analysis was carried out on time evolution data of the outward component of the Poynting vector, sampled along a semi-circle of radius 30 μm centered at the interaction point of the laser pulse and the target and extending on the rear side of the aluminum foil (see figure 4(b)). The radiation was frequency filtered with a bandpass filter centered at 60 ± 30 THz. The leading edge of the radiation front (time of arrival $t = 200$ fs) is characterized by a strong, asymmetric emission peak at $\theta = +53^\circ$ from the target normal (see figure 4(c), blue line). The emission lasts as little as 14 fs, revealing a broad frequency spectrum extending from the optical to THz frequencies. The radiation pattern can easily be modeled by the dipole emission associated with a bunch of electrons propagating at $\beta = \frac{v}{c} = 0.73$ (v is the velocity of the electron and c is the speed of light) along the direction of the incident heating pulse and deflected by an electric field normal to the target surface. Consistently, the charge diagnostic of the simulation revealed accordingly the presence of a negatively charged cloud propagating at $\beta = 0.75$ at $\theta = +21^\circ$ from the target normal.

At intermediate times of arrival ($230\,\text{fs} < t < 430\,\text{fs}$) a low-frequency emission ($f < 25$ THz) is observed in the simulation. The overall angularly resolved flux is plotted in figure 4(c) (green line), revealing a characteristic dipole emission symmetric around the target normal. The emission is peaked at angles of $\theta = \pm 47^\circ$ from the target normal, a value consistent with the emission of charged particles propagating at a speed of $\beta = 0.37$ parallel to the target normal, and accelerated along the same direction. The correspondingly modeled emission pattern is superimposed on the plot of figure 4(c) (dotted red line)[8]. The remarkable agreement of the model with the simulated radiation pattern suggests that a possible source of the non-collinear THz radiation is related to the dynamics of the TNSA mechanism. By irradiating a thin foil target with ultra-short laser pulses at intensities greater than 10^{18} W cm^{-2}, a population of extremely energetic hot electrons (several MeV) is generated. Some of these electrons travel through the target and escape at the rear surface, thereby generating a micron-scale plasma sheath with a space charge field of the order of TV m^{-1} [28, 29]. The sheath field is strong enough to field ionize the rear surface and accelerate protons and ions to very high energies.

[8] The non-collinearity of the T-rays was estimated using the angle of the Poynting vector lobes (figure 4(c)) with respect to the target normal. The angle between the radiation emission and the acceleration direction is defined by the formula $\theta_{\max} = \cos^{-1}[\frac{1}{3\beta}\sqrt{1+15\beta^2} - 1]$. Taking from the simulation the angle of 47°, the velocity of the accelerated particles can be estimated to be 0.37 times the speed of light.

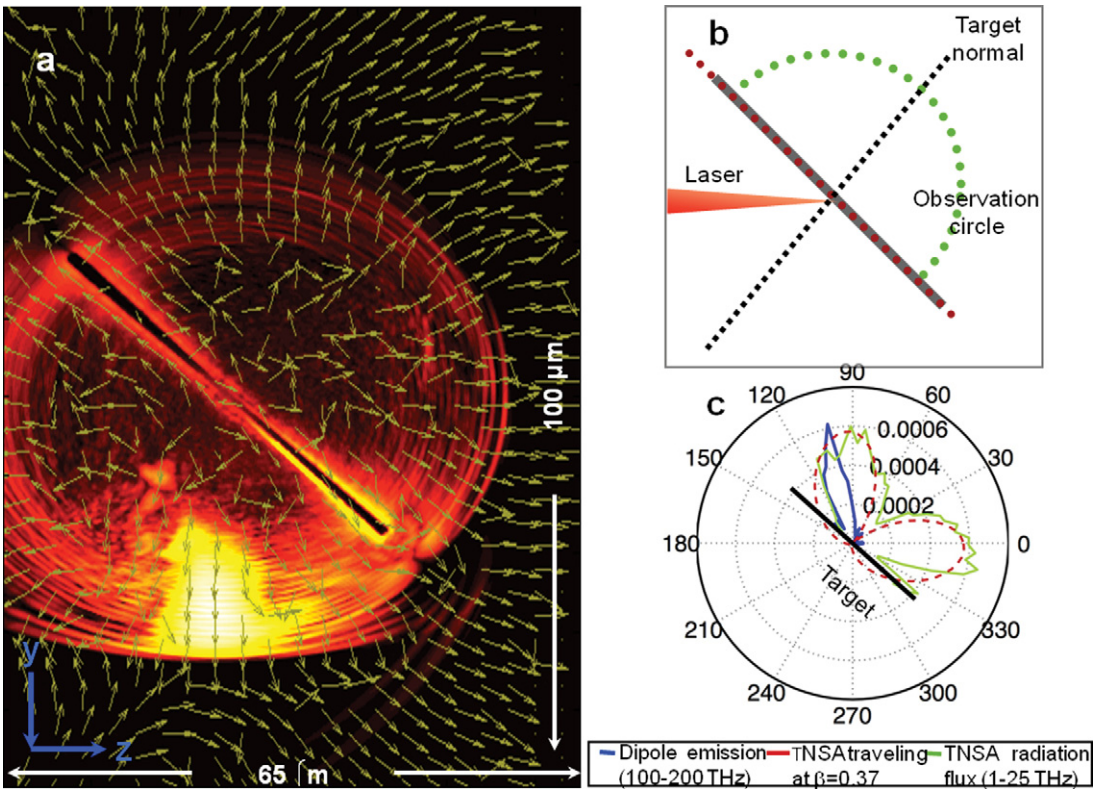

Figure 4. PIC simulation of the laser–plasma interaction. (a) A snapshot of the Poynting vector ($\mathbf{E} \times \mathbf{B}$) at time 194 fs from the beginning of the simulation. Overlaid arrows show the direction of energy flow. A significant part of the laser radiation which was impinging on the target front from the left has been reflected and is propagating downwards. (b) Schematic diagram of the simulation setup. Dotted green line represents an observation plane which covers a half circle of 30 μm radius from the center of the target rear surface. (c) The modulus of the Poynting vector is plotted along this observation plane. The blue line indicates angular distribution of the radiation flux (frequency filtered between 100 and 200 THz) passing through the observation plane. The green line indicates the radiation flux due to TNSA field (frequency filtered for < 25 THz and time gated between 230 and 430 fs). The dotted red line represents the expected dipole emission from accelerating particles traveling at $0.37c$ [27].

The energetic electrons leading the plasma sheath, which is of the order of a few microns, experience deceleration while the ions and protons are accelerated to several MeV energies. Because of the accelerating and decelerating dynamics of charged particles, radiation of electromagnetic waves is expected to be emitted according to a dipole-like pattern.

At later times ($t > 430$ fs), the radiation pattern is peaked at angles $\theta = +90^\circ$ from the target normal. The field snapshots clearly show that this radiation originates from a surface plasmon hitting the edge of the target, as reported previously by Sagisaka *et al* [19]. The low-frequency ($f < 25$ THz) time integrated flux across the observation plane shows that the emission is far from being uniform and most of the radiation is emitted off-axis with respect to the target

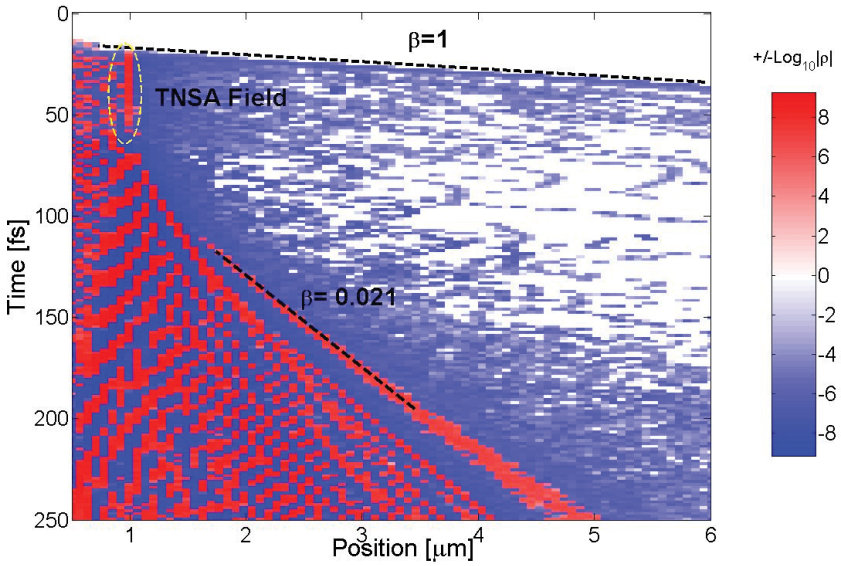

Figure 5. Net electric charge density as a function of the distance from the target and time. Blue: negative charge. Red: positive charge. The distance is measured from the rear surface along the normal direction from the center of the target.

normal. If the experiment was capable of detecting this emission, we would have observed that the flux passing directly through the aperture would represent 9.4% of the total collected radiation.

These three sources of THz radiation do not contribute on an equal footing to the experimentally observed emission. The contribution of the radiation generated by the deflected electrons fades rapidly at low frequencies, while a major contribution of the surface plasmon emission can be ruled out by the relatively large size of our target (3 cm). The excited plasmon is indeed expected to decay within a few mm of propagation, thus well before the edge of the foil is reached. The experimental setup indeed was capable of collecting only radiation emitted non-collinearly. Indeed, the angular distribution, polarization and the metal coin measurements indicate that the observed radiation is dipole like. This suggests that the target normal sheath acceleration (TNSA) emission could play a role in explaining the high yield of T-ray emission observed in the experiments. In fact, figure 5 is consistent with this conjecture. It shows the charge dynamics and distance at the center of the target rear surface over time. The zero time corresponds to the time the laser pulse hits the target. The ions (red) move more slowly compared to the electrons. The electrons escaping the rear surface develop a space charge field. Later on, the ions gain energy and get accelerated by the field generated by the charge separation. The charge separation drives the field and in turn leads to emission in the non-collinear direction.

3. Conclusions

In conclusion, the rich phenomenology observed in the simulation indicates that spatio-temporally resolved diagnostics of self-emitted THz radiation could be used to identify and monitor the acceleration of charged particles in relativistic plasmas. Various target geometries can be tested to obtain the contribution from the surface plasmons. Such diagnostics could

therefore be used to optimize both the laser-driven particle acceleration process and/or the generation of THz radiation. Using a laser-driven particle accelerator as a source of THz radiation could be promising; it is to be noted that the energy measured in our experiments was mainly in the off-axis direction and between 0.15 and 2 THz. According to the simulations, higher yields (up to $\times 10$) are expected in the 0.1–30 THz band, a value which would make the source competitive with other THz-generation methods. The average power of such a source depends on the repetition rate of the laser system, which in our case is 10 Hz, while the peak power is in the megawatt range, comparable with the existing synchrotron sources. The remarkable high energy of the T-ray pulses generated during relativistic laser–plasma interaction could find relevant applications in biological imaging and material science. Moreover, characterization of self-emitted T-rays has the potential of being a unique diagnostic for laser–plasma acceleration schemes, with relevance to the optimization of table-top laser-driven particle accelerators.

Acknowledgments

We thank H Ruhl for providing the Particle Simulation Code. AG acknowledges support from Carl-Zeiss-Stiftung. We also thank B Beleites and F Ronneberger for the smooth running of the JETI laser during the experiment and S Graef for running the CO_2 laser for the calibration of the pyroelectric detector.

References

[1] Ryutov D D *et al* 2001 Magnetohydrodynamic scaling: from astrophysics to the laboratory *Phys. Plasmas* **8** 1804
[2] Remington B A *et al* 1999 Modeling astrophysical phenomena in the laboratory with intense lasers *Science* **284** 1488
[3] Murnane M M *et al* 1991 Ultra-fast x-ray pulses from laser produced plasmas *Science* **251** 531
[4] Leemans W P *et al* 2006 GeV electron beams from a centimeter-scale accelerator *Nature Phys.* **2** 696
[5] Snavely R A *et al* 2000 Intense high-energy proton beams from petawatt laser irradiation of solids *Phys. Rev. Lett.* **85** 2945
[6] Macklin J J *et al* 1993 High-order harmonic generation using intense femtosecond pulses *Phys. Rev. Lett.* **70** 766
[7] Borghesi M *et al* 1998 Large quasistatic magnetic fields generated by a relativistically intense laser pulse propagating in a preionized plasma *Phys. Rev. Lett.* **80** 5137
[8] Kodama R *et al* 2001 Fast heating of ultrahigh-density plasma as a step towards laser fusion ignition *Nature* **412** 798
[9] Krushelnick K M *et al* 2002 Using self-generated harmonics as a diagnostic of high intensity laser-produced plasmas *Plasma Phys. Control. Fusion* **44** B233
[10] Tatarakis M *et al* 2002 Laser technology: measuring huge magnetic fields *Nature* **415** 280
[11] Watts I *et al* 2002 Dynamics of the critical surface in high-intensity laser–solid interactions: modulation of the XUV harmonic spectra *Phys. Rev. Lett.* **88** 155001
[12] Gopal A *et al* 2008 Temporally and spatially resolved measurements of multi-megagauss magnetic fields in high intensity laser-produced plasmas *Phys. Plasmas* **15** 122701
[13] Wagner W *et al* 2004 Laboratory measurements of 0.7 GG magnetic fields generated during high-intensity laser interactions with dense plasmas *Phys. Rev.* E **70** 026401

[14] Leemans W P *et al* 2003 Observation of terahertz emission from a laser–plasma accelerated electron bunch crossing a plasma–vacuum boundary *Phys. Rev. Lett.* **91** 074802
[15] van Tilborg J *et al* 2006 Temporal characterization of femtosecond laser–plasma accelerated electron bunches using terahertz radiation *Phys. Rev. Lett.* **96** 014801
[16] Kando M *et al* 2009 Experimental studies of the high and low frequency electromagnetic radiation produced from nonlinear laser–plasma interactions *Eur. Phys. J.* D **55** 465
[17] Reimann K 2007 Table-top sources of ultrashort THz pulses *Rep. Prog. Phys.* **70** 1597
[18] Hamster H *et al* 1993 Sub-picosecond, electromagnetic pulses from intense laser plasma interaction *Phys. Rev. Lett.* **71** 2725
[19] Sagisaka A *et al* 2008 Simultaneous generation of a proton beam and terahertz radiation in high-intensity laser and thin-foil interaction *Appl. Phys.* B **90** 373
[20] Li C *et al* 2011 Effects of laser–plasma interactions on terahertz radiation from solid targets irradiated by ultrashort intense laser pulses *Phys. Rev.* E **84** 036405
[21] Santos J J *et al* 2002 Fast electron transport in ultraintense laser pulse interaction with solid targets by rear-side self-radiation diagnostics *Phys. Rev. Lett.* **89** 025001
[22] Baton S D *et al* 2003 Evidence of ultrashort electron bunches in laser–plasma interactions at relativistic intensities *Phys. Rev. Lett.* **91** 105001
[23] Bellei C *et al* 2010 Micron-scale fast electron filaments and recirculation determined from rear-side optical emission in high-intensity laser solid interactions *New J. Phys.* **12** 073016
[24] Levongston S 2009 *Spectrum Detectors* http://www.gentec-eo.com/
[25] Gemuend H-P *et al* 1994 High-performance FIR bandpass filters for the ISOPHOT instrument *Proc. SPIE* **2268** 272
[26] Ruhl H and Mulser P 1995 Relativistic Vlasov simulation of intense fs laser pulse–matter interaction *Phys. Lett.* A **205** 388
[27] Jackson J D 1999 *Classical Electrodynamics* 3rd edn (New York: Wiley) chapter 14
[28] Romagnani L *et al* 2005 Dynamics of electric fields driving laser acceleration of multi-MeV protons *Phys. Rev. Lett.* **95** 195001
[29] Antici P *et al* 2008 Hot and cold electron dynamics following high-intensity laser matter interaction *Phys. Rev. Lett.* **101** 105004